





Article

Isotope Discrimination of Source Waters, Flowpaths, and Travel Times at an Acid-Generating, Lead–Zinc–Silver Mine, Silver Valley, Idaho, USA

Jeff B. Langman ^{1,*},[†] , Ethan Gaddy ^{1,†}, Timothy E. Link ² , Jan Boll ³ , Bradley Barnett ⁴ and Morgan Hill ⁴ 

¹ Department of Earth and Spatial Sciences, University of Idaho, Moscow, ID 83844, USA; gadd5510@vandals.uidaho.edu

² Department of Forest, Rangeland and Fire Sciences, University of Idaho, Moscow, ID 83844, USA; tlink@uidaho.edu

³ Department of Civil and Environmental Engineering, Washington State University, Pullman, WA 99164, USA; j.boll@wsu.edu

⁴ Bunker Hill Mining Corporation, Kellogg, ID 83837, USA

* Correspondence: jlangman@uidaho.edu; Tel.: +1-208-885-0310

[†] These authors contributed equally to this work.

Abstract: Precipitation infiltrates into the lead–zinc–silver Bunker Hill Mine, oxidizes pyrite, and produces acidic waters that discharge from the mine portal. The metasedimentary geology and alteration from 100+ yr of mining provide a heterogeneous environment for source water infiltration and flow within the mine. A university–industry partnership was developed to trace the mine water sources, flowpaths, and travel times to identify potential areas for infiltration reduction. Snowpack, creek, and mine water samples were collected over a 1-year period for the analysis of $\delta^2\text{H}$, $\delta^{18}\text{O}$, and ^3H , along with the in situ measurement of temperature, specific conductance, pH, dissolved oxygen, and flow. The isotope tracers were used to identify the source waters, unmix mine water as it moved deeper in the mine, and examine flowpaths in and near the acid-generating pyritic zone. The results indicate creek water infiltrating relatively quickly through the anthropogenically-modified pathways and causing the largest amount of acidic water in the upper levels of the mine. Slower, natural pathways associated with faults, fractures, and bedding planes produce mostly neutral waters with the source waters typically originating at higher elevations. Travel times ranged from <1 to 22 years with shorter pathways to the upper levels of the mine and increasing contributions deeper in the mine from pathways containing older, higher-elevation snowmelt. These slower and older inflows were identified by depleted $\delta^{18}\text{O}$ values, smaller ^3H concentrations, the dampening of the variability of the isotope signals, and pH increases. Reduction of infiltration zones near the upper workings of the mine likely will decrease the acidic waters in the upper levels of the mine, but the higher elevation infiltration zones will continue to contribute snowmelt-derived waters at all mine levels.



Citation: Langman, J.B.; Gaddy, E.; Link, T.E.; Boll, J.; Barnett, B.; Hill, M. Isotope Discrimination of Source Waters, Flowpaths, and Travel Times at an Acid-Generating, Lead–Zinc–Silver Mine, Silver Valley, Idaho, USA. *Water* **2023**, *15*, 3362. <https://doi.org/10.3390/w15193362>

Academic Editor: Liliana Lefticariu

Received: 31 July 2023

Revised: 15 September 2023

Accepted: 19 September 2023

Published: 25 September 2023

Keywords: water isotopes; pyrite oxidation; mine water; acid rock drainage



Copyright: © 2023 by the authors. Licensee MDPI, Basel, Switzerland. This article is an open access article distributed under the terms and conditions of the Creative Commons Attribution (CC BY) license (<https://creativecommons.org/licenses/by/4.0/>).

1. Introduction

The generation of acid rock drainage (ARD) from abandoned mines can severely impact local and regional water resources [1–3]. In the United States, the release of ARD from abandoned mines has led to substantial environmental degradation [4–6]. In the Coeur d’Alene Mining District of northern Idaho (Silver Valley), the Bunker Hill Mine (Figure 1) is well known for its argentiferous galena [PbS] and sphalerite [(Zn,Fe)S] deposits. Associated with this ore is a large pyrite [FeS₂] deposit (pyritic zone) (Figure 2), which has caused ARD to discharge from the mine since industrial production began in the late 19th century. Infiltrating precipitation from the mountains oxidatively dissolves the pyrite, generates acid, mobilizes metals and sulfur, and discharges from the mine’s main

portal (Kellogg Tunnel, Figures 2 and 3) [7]. The ARD exiting the mine portal requires continuous collection and treatment at a water treatment plant in the adjacent town of Kellogg (Figure 1). The University of Idaho and the new mine owner (Bunker Hill Mining Corporation) formed a university–industry partnership to evaluate the sources, flowpaths, and travel times of the mine water through analysis of the stable and radiogenic isotopes of the water ($\delta^2\text{H}$, $\delta^{18}\text{O}$, and ^3H) to provide relevant information for targeting surface and subsurface areas for infiltration reduction. The application of the isotope tracers to this mine water issue is in response to prior hydraulic and solute tracer studies [7,8] that have been unable to fully resolve the source waters responsible for the ARD.

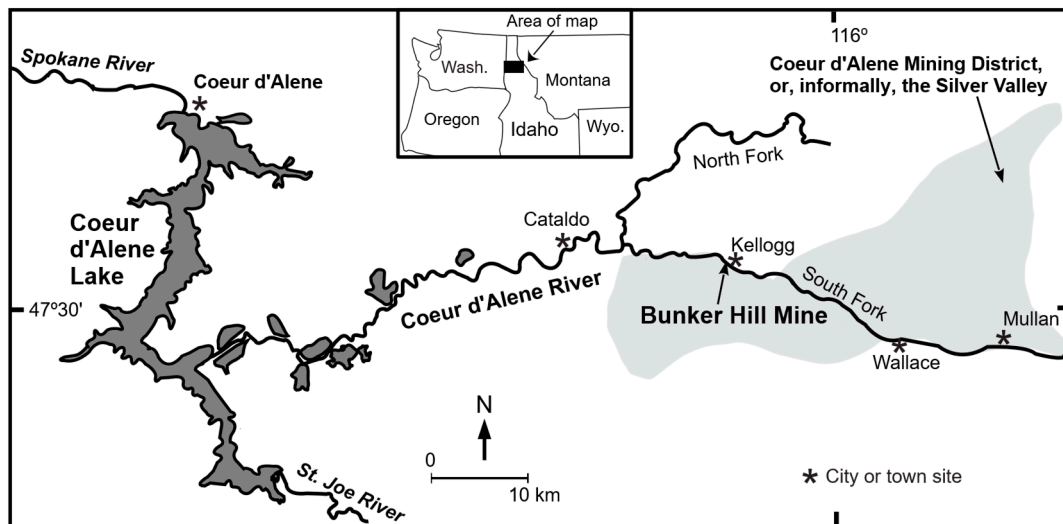


Figure 1. Location of the Bunker Hill Mine in the Coeur d’Alene Mining District in the Coeur d’Alene River Basin, Idaho, USA.

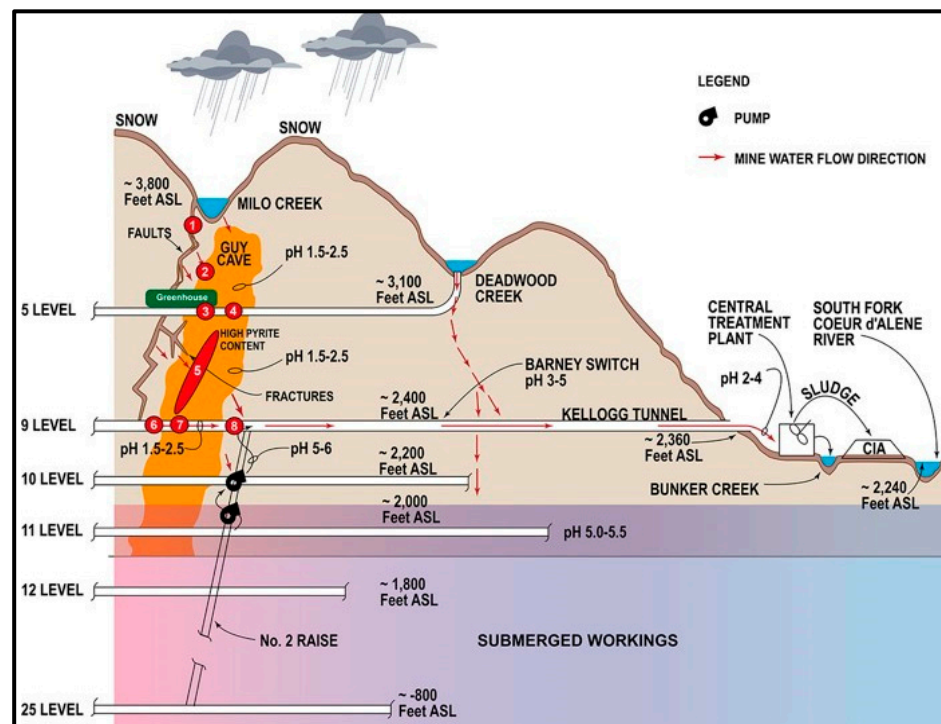


Figure 2. Simplified cross-section of the Bunker Hill Mine and the likely pathways of infiltrating precipitation into the color-coded pyritic zone (from Germon et al. [8], courtesy of the Bunker Hill Mining Corporation). Only select mine levels are presented. Figure not to scale.



Figure 3. Acidic and metal-rich mine water discharging (channel along the cement berm) from the Bunker Hill Mine portal (Kellogg Tunnel).

1.1. Basin and Mine Geology

The Silver Valley is contained in the upper portion of the Coeur d'Alene River Basin (Figure 1), which is composed of quartzites, argillites, and siltites of the Mesoproterozoic Belt Supergroup that have been uplifted, folded, and fractured [9–13]. The Osburn Fault runs the length of the valley and is the origin of the NW-SE trending, strike-slip splay faults, such as the Alhambra, Cate, and Midland faults, that dip steeply southward through the mine site (Figure 4). These faults are the primary locations of the Bunker Hill galena–sphalerite ore [14–16] deposited from repeated Mesoproterozoic to Cretaceous hydrothermal intrusions [10,11,13].

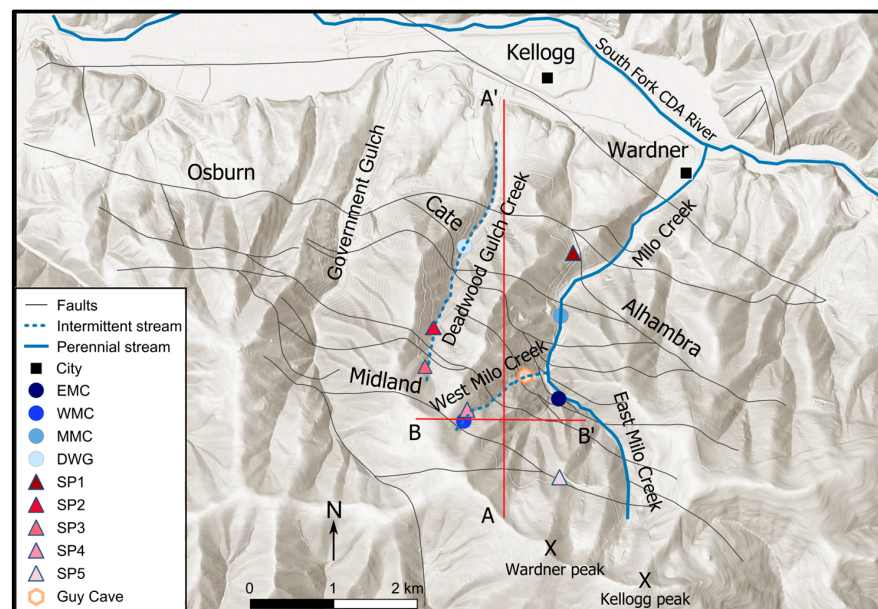


Figure 4. Surface sampling locations, Guy Cave, faults, creeks, and the South Fork of the Coeur d'Alene (CDA) River near the Bunker Hill Mine, Idaho, USA (adapted from Idaho Geological Survey *Geologic Map of Idaho*, ESRI hillshade basemap). Creek sampling locations include East Milo Creek (EMC), West Milo Creek (WMC), the main stem of Milo Creek (MMC), and Deadwood Gulch Creek (DWG). Snowpack sampling locations (SP1 to SP5) differ by elevation ranging from 1015 m to 1543 m NAVD 88. Cross section indicators are relevant to Figure 13.

The upper Revett Formation of the Belt Supergroup is the primary ore-containing formation at the mine site and is comprised of quartzite beds interbedded with layers of argillite and siltite [13]. The hydrothermal intrusions invaded the faults and fractures of the steeply dipping quartzite beds that emplaced the galena–sphalerite ore along with substantial pyrite [10,11,13]. Pyrite is associated with the ore deposits of the Silver Valley, but it is commonly found with substantial acid-neutralizing carbonate deposits, such as siderite [FeCO₃] and ankerite [Ca(Fe,Mg,Mn)(CO₃)₂] [9,17]. At the Bunker Hill Mine, pyrite is found in greater abundance, and there are limited carbonate deposits near the pyritic zone in the upper portion of the mine [9,17,18].

1.2. Mine Water in the Upper Workings

The upper workings of the Bunker Hill Mine (Figure 2) are located beneath Kellogg and Wardner peaks of the Coeur d'Alene Mountains and extend from Government Gulch across to the Milo Creek watershed (Figure 4). This upper portion of the mine contains complex fold and fault systems [9,12,13], and the area has been heavily mined since the 1880s. The combination of steeply dipping bedding planes, extensive mine workings, thousands of unplugged drillholes, and highly fractured and faulted stratigraphy has resulted in a complex system for the transport of infiltrating water derived from snowmelt in the surrounding mountains [14,16,19]. Numerous infiltration zones are located at the mine site because of the geologic characteristics and mining activity, including a block caving area (Guy Cave, Figure 4), which caused subsidence of the land surface and additional fractures for the entrance of infiltrating water [20]. Additionally, a portion of the depression caused by the block caving was filled with pyritic waste rock.

Snow comprises the majority of precipitation [21], which, combined with the steep terrain, results in a dominant runoff period during the spring snowmelt (Figure 5). Prior investigations have identified increased mine water during the spring snowmelt, which constitutes the primary groundwater/mine water recharge period [7,21–23]. Likely infiltration zones are associated with Milo Creek and its tributaries (East Milo Creek and West Milo Creek), Guy Cave, and Deadwood Gulch Creek (Figure 4) [7,23,24]. Historically, the spring snowmelt and increased mine water volume generated greater acidic water in the mine [23]. Lachmar [7] suggested that the bedding planes, brecciated faults, and major joints of the Revett Formation are the primary pathways of groundwater flow, and mining enhanced the connections between these pathways, particularly the new fractures created from block caving [14,20,23,25]. Much of the flow of West Milo Creek has been observed to be lost to infiltration in the vicinity of Guy Cave [14,20], and it has been suggested that a substantial portion of flow in East Milo Creek infiltrates into the underlying fault system and mine workings [14,19,20]. A prior tracer study found substantial spring/summer increases in mine water in the upper workings that moderated with further travel into the lower levels [14,19].

1.3. Water Isotopes and Source Waters

The stable and radiogenic isotopes of water ($\delta^2\text{H}$, $\delta^{18}\text{O}$, and ^3H) are primary tools for discriminating groundwater sources, flowpaths, and travel times and can be effective tracers in chemically reactive systems where traditional geochemical analytes may be ineffective [26–30]. Snow $\delta^2\text{H}$ and $\delta^{18}\text{O}$ values typically are depleted compared to non-snow precipitation because of the isotopic lapse rate [31,32]. Ablation of a snowpack can increase the presence of heavier isotopes [33,34], but snowpack/snowmelt sources commonly provide traceable, depleted $\delta^2\text{H}$ and $\delta^{18}\text{O}$ signals compared to rainfall [35–37]. Additionally, snow $\delta^2\text{H}$ and $\delta^{18}\text{O}$ values will vary according to elevation [38], which allows for the discrimination of higher or lower elevation snow/snowmelt [39]. With greater distance of overland flow, snowmelt $\delta^2\text{H}$ and $\delta^{18}\text{O}$ values typically will become enriched relative to the depleted snow signal because of evaporation, which can allow for the discrimination of quickly infiltrating snowmelt or downgradient infiltration from overland flow [33,34]. A study by Sánchez-Murillo et al. [40] in a sub-basin near the Bunker Hill

Mine found significant seasonal variability of $\delta^2\text{H}$ and $\delta^{18}\text{O}$ values for precipitation and creek water (e.g., precipitation $\delta^{18}\text{O}$ of -22.7‰ to -6.7‰ and creek $\delta^{18}\text{O}$ of -16.2‰ to -14.5‰), the most depleted $\delta^{18}\text{O}$ values in winter precipitation, and the most depleted creek $\delta^{18}\text{O}$ values from winter to spring.

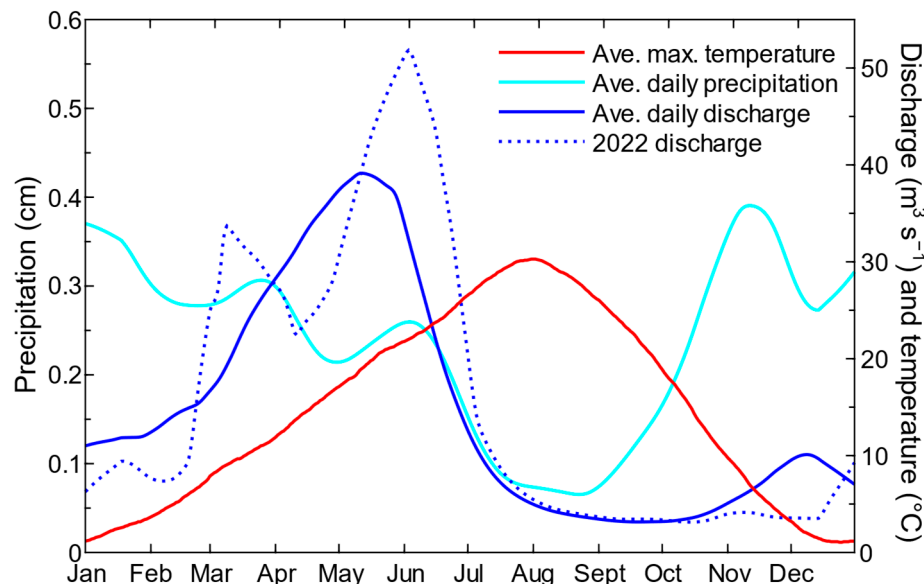


Figure 5. Lowess trend lines of discharge during the study period and average discharge of the South Fork of the Coeur d’Alene River (1986–2023, US Geological Survey station 12,413,470 near Pinehurst, Idaho) and average precipitation (1991–2020) and maximum temperatures (1981–2010) for Kellogg, Idaho (Western Regional Climate Center climate summaries for Kellogg, Idaho).

The short half-life of ^3H makes it an effective tool for evaluating travel time in most shallow groundwater systems [22,41]. Tritium is naturally produced in the stratosphere through cosmic ray spallation of nitrogen and oxygen [42]. Modern atmospheric ^3H concentrations are considered to have returned to pre-bomb levels, although high latitudes of the northern hemisphere can be enriched in ^3H relative to the global average [41,43]. Precipitation in the northern latitudes can be seasonally enriched in ^3H because of the “spring leak” from the stratosphere [44]. The spring leak consists of a temporary migration of the tropopause upward from winter to spring, leading to the incorporation of the lower stratosphere into the air currents typically isolated to the troposphere [22]. As the stratosphere is the largest reservoir of ^3H , the spring leak increases ^3H concentrations in winter/spring precipitation in the northern latitudes [22]. Sites in the western USA have observed increased ^3H in precipitation and snowpack in winter through spring [45–47], which corresponds to the primary precipitation period of the study site (Figure 5).

2. Methods

A sampling network was established at the Bunker Hill Mine to collect snow, surface water, and mine water over a 1-yr period for the analysis of $\delta^2\text{H}$, $\delta^{18}\text{O}$, and ^3H . Sampling was conducted on a twice-monthly basis between 15 June 2021 and 29 June 2022. The goal of the snow and creek sampling was to determine relative spatial and temporal differences in the isotope values of likely source waters that could infiltrate into the mine. The collection of mine water was conducted to correlate the likely source waters and the connections between mine levels that contribute to the acidic water discharging from the mine portal.

2.1. Snow Sampling

Five snow sites (SP1–5 with respective elevations of 1015, 1198, 1338, 1460, and 1543 m NAVD 88, Figure 4) in the Milo Creek and Deadwood Gulch watersheds (aligned along the access road to Wardner Peak) were sampled from December 2021 to May 2022. Snow

sampling sites were chosen to minimize the collection of disturbed snow as well as snow redistributed by canopy throughfall and slumping from the upgradient snowpack. Snow sampling consisted of the collection of a composite (top to base of the snowpack) and base layer (bottom 0.15 m of the snowpack) sample at each site to evaluate the isotopic differences by elevation and within the snowpack (base layer as potential snowmelt indicator). For the collection of the composite and base layer samples during shallower snowpacks (<1.5 m), the samples were collected by trenching and scraping the open face with a trowel (Figure 6). During deeper snowpacks, an adjustable-length, 7.5-cm diameter, aluminum coring device was used to collect snow samples through the insertion of the coring device from the top to base of the snowpack. All snow samples were vacuum sealed in 1-L bags and returned to the mine laboratory, where the samples were placed in an oven at approximately 25 °C. Following the melting of the snow samples in the sealed bags, the resulting water was syringe filtered (1 µm) into 125 mL ($\delta^2\text{H}$ and $\delta^{18}\text{O}$) and 500 mL (^3H) HDPE containers (no headspace) and sealed with polyseal caps.



Figure 6. Snowpack trench at sample site SP2 at an elevation of 1198 m NAVD 88.

2.2. Creek Sampling

Surface-water sampling sites (East Milo Creek (EMC), West Milo Creek (WMC), the main stem of Milo Creek (MMC), and Deadwood Gulch (DWG) (Figure 4) were established to evaluate the isotopic signals of surface water near the upper mine workings. The surface water samples were collected as unfiltered, depth-integrated samples in 125 mL ($\delta^2\text{H}$ and $\delta^{18}\text{O}$) and 500 mL (^3H) HDPE containers (no headspace) and sealed with polyseal caps. Due to the intermittent nature of WMC and DWG, these sites were unavailable for sampling during the late summer/early fall portion of the study period.

2.3. Mine Water Sampling

Fourteen mine water sampling sites were established on the mine's 5 to 9 levels (Figure 2) that encompass the upper pyritic zone (no access to the levels above the 5 Level).

The mine water sites are referenced by their level (first numeral) and stope description (2–3 alphanumeric) (Table 1). The mine water samples were collected from drainages in the stopes (Figure 7) as unfiltered, depth-integrated samples in 125 mL ($\delta^2\text{H}$ and $\delta^{18}\text{O}$) and 500 mL (^3H) HDPE containers (no headspace) and sealed with polyseal caps. Due to site access restrictions, sites 5WM and 5BK were incorporated into the sampling two months after the start of sampling and site 7KX after the first month. Access to 5AO was suspended near the end of the study due to mine restart activities.

Table 1. Sampling sites and their relative location to the pyritic zone in the Bunker Hill Mine.

Site Name	Site Identifier	Mine Level	Elevation (m, NAVD 88)	Relation to Pyritic Zone
East Milo Creek	EMC	surface	1024	above
West Milo Creek	WMC	surface	1390	above
Milo Creek, main stem	MMC	surface	866	adjacent
Deadwood Gulch	DWG	surface	1084	above
Greenhouse 2 Reed Drift	5GH2	5	945	internal
Becker Flume	5BK	5	943	external
Williams Raise	5WM	5	943	external
Asher Ore Chute	5AO	5	954	transition
Crusher Station	6CS	6	892	internal
Cherry Raise 7	7CR	7	844	external
Flood Drifts	7FL	7	857	internal
Kateye Crosscut	7KX	7	845	external
Cherry Raise 8	8CR	8	786	external
Van Raise	9VR	9	737	external
Bailey Ore Chute	9BO	9	737	external
Stanly Crosscut	9SX	9	733	internal
South Chance	9SC	9	732	external
Hite Drift	9HD	9	734	external

Note: Site identifiers contain a numeral corresponding to the mine level followed by a two-letter abbreviation corresponding to the stope. Relation to the pyritic zone is relative to the presence of acidic waters in areas known to contain substantial pyrite. Elevation is relative to the North American Vertical Datum 1988 (NAVD 88).

2.4. Field Parameter and Laboratory Analyses

At each creek/mine sampling location, a calibrated Hanna multiparameter probe (HI98130) was used to measure temperature ($\pm 0.1^\circ\text{C}$), specific conductance ($\pm 0.01\text{ mS cm}^{-1}$), and pH ($\pm 0.01\text{ pH}$). For quality-control purposes, a randomly selected site was designated for duplicate sample collection during each sampling period. Discharge at the creek and mine sites was determined using a Hach FH950 portable velocity meter ($\pm 0.015\text{ m s}^{-1}$) at naturally occurring cross sections. Stable isotope ratios were analyzed at the University of Arizona with a Finnigan Delta S gas source isotope ratio mass spectrometer (precision of $\pm 0.9\text{‰}$ for $\delta^2\text{H}$ and $\pm 0.08\text{‰}$ for $\delta^{18}\text{O}$) using the methods described by Lu [48]. Tritium analyses were performed at the University of Arizona with a Quantulus 1220 Spectrometer. The samples were distilled to remove non-volatile solutes, enriched by electrolysis, then mixed 1:1 with an Ultima Gold Low-Level Tritium (R) cocktail. The samples were placed in the spectrometer in an underground laboratory for a 1500 min counting period. Under these conditions, the ^3H detection limit is a 0.5 tritium unit (TU), the standardization is relative to NIST SRM 4361C, and the background value was determined from the Pleistocene water taken from a well in the Tucson Basin [49].

2.5. Deuterium Excess, Evaporation, and Vapor Recycling

Deuterium excess (d-excess) values were used to identify a potential influence on source water isotope values because of pyrite oxidation (exothermic reaction). Evaporation of the waters within the pyritic zone was of concern because this area can contain warm, stagnant air masses where the relative humidity is often above 90%. D-excess is a second-order stable isotope parameter (d-excess = $\delta^2\text{H} - 8 \times \delta^{18}\text{O}$) that can indicate evaporation and vapor sources [40,50,51]. The d-excess values were examined to identify whether pyrite

oxidation was causing substantial evaporation, thereby altering stable isotope values [52,53]. An adjustment factor was determined for the affected sites by comparing their d-excess values to the unaffected sites (e.g., internal vs. external pyritic zone sites).



Figure 7. Sampling of mine water at the pyritic zone site 5GH2, Bunker Hill Mine (Pictured: Morgan Hill, Bunker Hill Mining Corporation).

2.6. Conceptual Model and Isotope Unmixing

To evaluate the source water mixing in the mine, a conceptual model of potential flowpaths was derived from the field parameter values, previously published literature (e.g., tracer tests and fault orientations), discharge observations, and the $\delta^{18}\text{O}$ values of the potential source waters (e.g., snowpack, creek water, or upper-level mine water). A snowpack source was assigned as the median $\delta^{18}\text{O}$ value of the uppermost site (SP5) because its isotope range encompassed a relatively depleted source that also evolved given the five months it was present on the mountain. Creek water sources were assigned as median $\delta^{18}\text{O}$ values of the higher elevation sources (WMC and EMC), or an evaporated source (DWG) that could represent more isotopically depleted source waters infiltrating near Guy Cave (WMC and EMC) or a more evolved (evaporated) overland source (DWG). The snowpack and creek water $\delta^{18}\text{O}$ values were evaluated as likely source waters for the 5-Level sites, and the lower-level mine sites were evaluated for potential sources from the upper levels or from the snowpack source. The $\delta^{18}\text{O}$ values of the selected source waters were used for two-component unmixing (inverse modeling) using Equation (1). The inverse calculation allows for the unmixing of mine water isotope values (δ_m) by varying the possible fractions (f_1, f_2) of the selected source water isotope values (δ_1, δ_2). Microsoft Excel (Goal Seek) was used to perform the inverse calculations. The inverse calculation is a best-fit scenario where the fractions of likely source waters are varied concurrently to

minimize the residual of the model solution compared to the actual $\delta^{18}\text{O}$ value. The output of the inverse modeling was a percent contribution of the perceived source waters at each mine water sampling site over the duration of the study.

$$f_1\delta_1 + f_2\delta_2 = \delta_m \quad (1)$$

2.7. Tritium and Travel Time

The modern method of $^3\text{H}/^3\text{He}$ dating was not applicable for estimating mine water age (travel time (t)) because of the atmospheric influence within the mine workings. With the inability to use ^3He in conjunction with ^3H , an initial ^3H value ($^3\text{H}_0$) was selected as the average of the spring season snowpack for all sites (4.5 TU or the 62.5 percentile of ^3H distribution for the entire snowpack season), which also is the median value of the DWG creek water ^3H distribution. This $^3\text{H}_0$ is greater than nearly all the values recorded for mine water except for two samples at 5 BK (concentrations of 4.75 TU) that appear to have captured high elevation snowmelt. The lower 4.5 TU value for $^3\text{H}_0$ was selected because it aligned with the median value of DWG that responds only to snowmelt and runoff (intermittent stream) and was similar to the mean value of the snowpack at all snow sampling sites between February and May (largest snowpack period). Values > 4.5 TU were assumed to be recent recharge (< 1 yr). The resulting ages are a relative estimate of travel time given the assumption of the dominance of the ^3H -enriched snowmelt in winter and spring that recharge the infiltration areas each year. Mine water travel times (Equations (2) and (3)) were estimated from the decay of ^3H ($^3\text{H}_t$) given the selected $^3\text{H}_0$. A decay constant (λ) of 0.05626 was used for the travel time calculations given the ^3H half-life of 4500 d [54].

$$^3\text{H}_t = ^3\text{H}_0 e^{-\lambda t} \quad (2)$$

$$t = \frac{-\ln\left(\frac{^3\text{H}_t}{^3\text{H}_0}\right)}{\lambda} \quad (3)$$

2.8. Trend Lines

Trend lines of temporal data were created using the Lowess (locally weighted scatterplot smoothing) technique (three iterations, $f = 0.2$ (smoother span)) to better characterize temporal trends by reducing the influence of outliers in the data. This nonparametric regression technique produces a line of central tendency to visually assess the relation between two variables.

3. Results

3.1. Source Waters and Mine Water Characteristics

Given the potential cold temperature of the infiltrating snowmelt, temperature variability of the mine water can be an indicator of the source waters and their temporal changes in contribution [55]. Mine water temperatures (Figure 8) may not directly reflect the temperature of the source waters (e.g., snowmelt or creek water) because of the potential alteration from pyrite oxidation (exothermic reaction) [56] and the high geothermal gradient of the region (estimated 1.8 °C per 100 m [57]). Warren [57] indicated the substantial variation in mine water temperatures at Bunker Hill and strongly increasing temperatures with depth—an estimated increase of 0.8 °C per 30 m in the lower levels of the mine. Groundwater in the upper mine workings should not experience such strong temperature increases from the geothermal gradient because of the atmospheric influence on mine air from the multitude of portals and adits that were created during the 100+ years of mining—240 km of tunnels and 9.6 km of inclined shafts, raises, and winzes [19]. Although, an area on the 5 Level in the pyritic zone was used as a greenhouse because of continuously warm and humid conditions [58]. Mine water that is relatively cold (e.g., 5WM in Figure 8) likely reflects the entrance of more direct snowmelt to flowpaths that feed these sites, while warmer mine water (e.g., 5GH2 in Figure 8) likely reflects warmer source waters—longer

overland flowpaths and/or pyrite oxidation/geothermal warming. Sample sites with highly variable mine water temperatures are indicative of shorter, responsive flowpaths from recharge sources, such as 5GH2 and 6CS that varied by 7 and 10 °C, respectively (Figure 8). Sample sites exhibiting less temperature variation (<2.5 °C: 5WM, 7KX, 9SC, and 9SX) likely are reflective of longer flowpaths, where temperature is a balance of the source water temperature and the exothermic reactions/geothermal gradient.

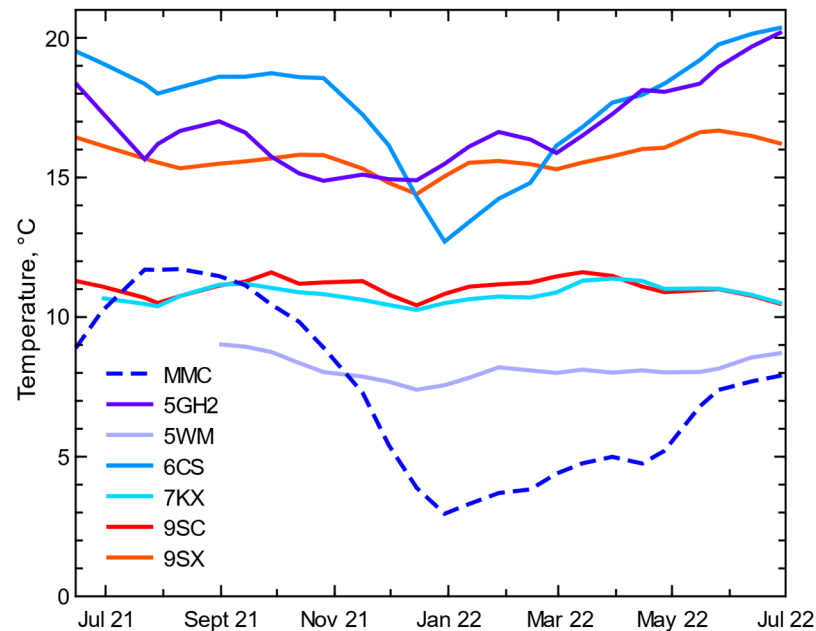


Figure 8. Lowess trend lines of water temperature at Milo Creek (MMC) and select mine water sampling sites on the 5, 6, 7, and 9 levels of the mine.

The pH and specific conductance of mine water substantially varied by sample site because of the differences in flowpaths that intersected, or did not intersect, the pyritic zone (Figure 9). Mine water sites 5GH2, 6CS, and 7FL contained the poorest water quality with pH ranging from 1.5 to 2.8 and specific conductance ranging from 10 to 20 mS cm⁻¹. Site 9SX contained water with lower specific conductance values (4 to 10 mS cm⁻¹) but acidic conditions (pH of 1.7 to 2.5). Sites containing water with pH > 3 and specific conductance values < 2 mS cm⁻¹ (5WM, 5BK, 7KX, 9SC, 9VR, 9BO, and 9HD) appear to have flowpaths that do not substantially intersect the pyritic zone and more closely resemble the creek water conditions (pH > 5, <1 mS cm⁻¹). The break in water quality associated with water at pH near 3 aligns with strong acid generation during the oxidation of pyrite and the increased mobility of metals, such as Fe and Mn, with pH < 3.5 and oxic/hypoxic conditions (5-Level mine water contained 1.5 to 9 mg/L O₂) [59]. Sites 9SC and 9HD contained water of relatively good quality (pH > 6, specific conductance < 1 mS cm⁻¹) similar to surface waters, which indicate source water pathways that are isolated from mine workings and the pyritic zone until emergence on the 9 Level.

3.2. Isotopes and Source Waters

The snowpack δ²H and δ¹⁸O values ranged from −143.0‰ to −112.6‰ for δ²H and −19.2‰ to −15.0‰ for δ¹⁸O, and the creek values ranged from −116.5‰ to −104.3‰ for δ²H and −15.9‰ to −13.9‰ for δ¹⁸O (Figure 10). The snow and creek δ²H and δ¹⁸O values plot along a local meteoric water line (LMWL: δ²H = 6.8 × δ¹⁸O − 9.2, R² = 0.87) indicative of evaporation effects compared to the global meteoric water line (GMWL) (Figure 10). The snowpack base samples were more depleted than the snowpack composite samples, with a median of −17.6‰ for δ¹⁸O in the snowpack base and a median of −17.3‰ for the snowpack composite samples. The mine water δ²H and δ¹⁸O values ranged from −124.1‰ to −102.8‰ for δ²H and −16.0‰ to −13.6‰ for δ¹⁸O. Most mine water samples had stable

isotope values similar to the range of creek values, although select sites on the 5 and 6 levels (5GH2, 5AO, and 6CS) contained water with isotope values that were more enriched than the creek values, and 9SC contained water more depleted than the creeks. Sites on the 5 Level contained water with the largest range of $\delta^2\text{H}$ and $\delta^{18}\text{O}$ values reflective of the likely shorter flowpaths from nearby surface water sources. These potential shorter flowpaths to the 5 Level have been theorized by past investigators [23] and mine personnel because of the disappearance of West Milo Creek near the Guy Cave and loss from East Milo Creek.

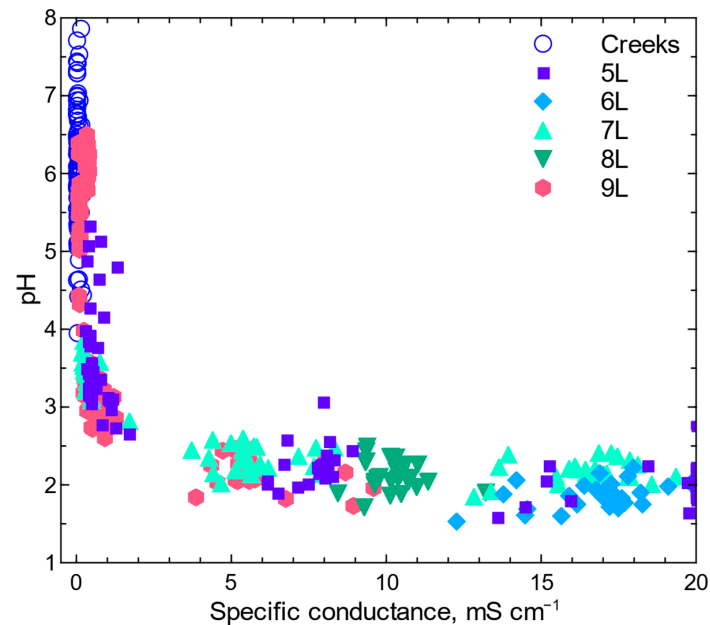


Figure 9. Specific conductance and pH of creek and mine water at the study site. Deadwood Gulch and Milo Creek sampling sites have been compiled under “Creeks” and mine water sites have been grouped by level (“5L” = 5 Level).

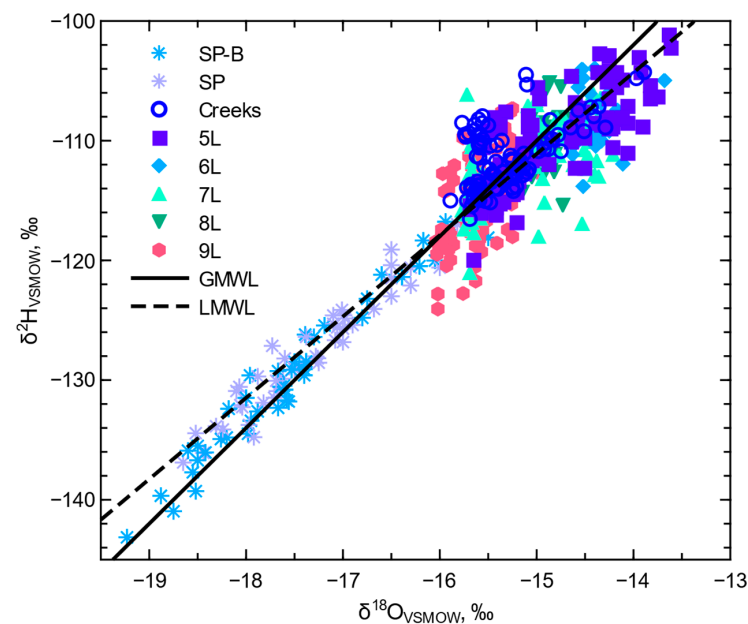


Figure 10. $\delta^2\text{H}$ and $\delta^{18}\text{O}$ values for snowpack, creek water, and mine water collected at the study site. Snowpack values were separated into the composite (SP) and base (SP-B) samples, while creek water (Deadwood Gulch and Milo Creek watersheds) results were compiled under “Creeks”. The global meteoric water line (GMWL: $\delta^2\text{H} = 8 \times \delta^{18}\text{O} + 10$) is pictured alongside the observed local meteoric water line (LMWL: $\delta^2\text{H} = 6.8 \times \delta^{18}\text{O} - 9.2$) derived from creek water and snowpack values.

Mine water from the 5 Level typically contained water with relatively enriched $\delta^2\text{H}$ and $\delta^{18}\text{O}$ values, although the 5 Level water indicated the largest range of values (e.g., -15.7‰ to -13.6‰ for $\delta^{18}\text{O}$). Water from the 9 Level contained the most depleted and smallest range of $\delta^2\text{H}$ and $\delta^{18}\text{O}$ values (e.g., -16.0‰ to -15.1‰ for $\delta^{18}\text{O}$). The change from mine water with relatively enriched isotope signals at the 5 Level to the depleted isotope signals of the 9 Level suggests isotopically enriched, lower elevation water (e.g., overland runoff) entering the upper mine levels then mixing with isotopically depleted water that infiltrated at higher elevations (e.g., isotopically depleted, high elevation snowmelt). This indicator of higher elevation, infiltrated snowmelt that bypasses the pyritic zone aligns with the elevation-isotope gradient in the $\delta^2\text{H}$ and $\delta^{18}\text{O}$ values of the base of the snowpack where the highest elevation site had the most depleted $\delta^2\text{H}$ and $\delta^{18}\text{O}$ values (average of -131.5‰ and -17.8‰ , respectively) and the lower elevation snowpack sites had more enriched $\delta^2\text{H}$ and $\delta^{18}\text{O}$ values (average of -129.7‰ and -17.5‰ , respectively). The elevation trend of depleted to enriched isotope values also was visible between the upper elevation Milo Creek sites of EMC and WMC (average $\delta^{18}\text{O}$ of -15.5‰) that contained slightly more depleted values compared to the lower elevation main-stem Milo Creek site (average $\delta^{18}\text{O}$ of -15.4‰ for MMC). The Deadwood Gulch site had an average $\delta^{18}\text{O}$ of -14.5‰ , which is reflective of the lower elevation of this watershed compared to the Milo Creek watershed and the slower creek flow in Deadwood Gulch. The down-level mixing in the mine with the introduction of more isotopically depleted water lower in the mine produces the variable water quality with poor water quality derived from the water passing through the pyritic zone and better water quality in the flowpaths outside of the pyritic zone that may have originated at upper elevation infiltration zones. Such a mixing pattern is visible in the temporal trends of $\delta^{18}\text{O}$ values for the mine water sites (Figure 11) where temporal variability decreases (e.g., longer flowpaths) and the $\delta^{18}\text{O}$ values become more depleted moving deeper into the mine. The more similar $\delta^{18}\text{O}$ values for the mine water on the 9 Level indicate a larger contribution of the high elevation snowmelt to the mine water exiting at this level.

Although the 5 Level sites were typically more temporally reactive and isotopically enriched compared to the lower levels (Figure 11), sites 5WM and 5BK contained mine water with relatively depleted $\delta^{18}\text{O}$ values (average of -15.5‰ and -15.2‰ , respectively) and relatively better water quality ($\text{pH} > 3$ and conductivity $< 2 \text{ mS cm}^{-1}$). Additionally, these sites exhibited less temporal isotopic variation (Figure 11). The results for 5WM and 5BK suggest a substantial portion of the mine water at these sites is derived from the flowpaths outside of the pyritic zone and may contain a higher elevation, infiltrated snowmelt that more slowly enters the mine. Moving lower into the mine, the water from subsequent levels indicated more depleted $\delta^{18}\text{O}$ values and less temporal variation (Figure 11). Although, each subsequent level contains sites that were temporally reactive + isotopically enriched or less reactive + less enriched. This separation of sites according to the temporal reactivity of their stable isotope signal suggests a primary separation of shorter flowpaths from the surface through or near the pyritic zone and potentially longer flowpaths from higher elevation infiltration zones. Yet, moving deeper into the mine lessens these differences, suggesting greater contributions from flowpaths outside of the pyritic zone (better water quality) bringing in higher elevation water (more depleted isotope signal) that slowly enters the mine (less temporal variation).

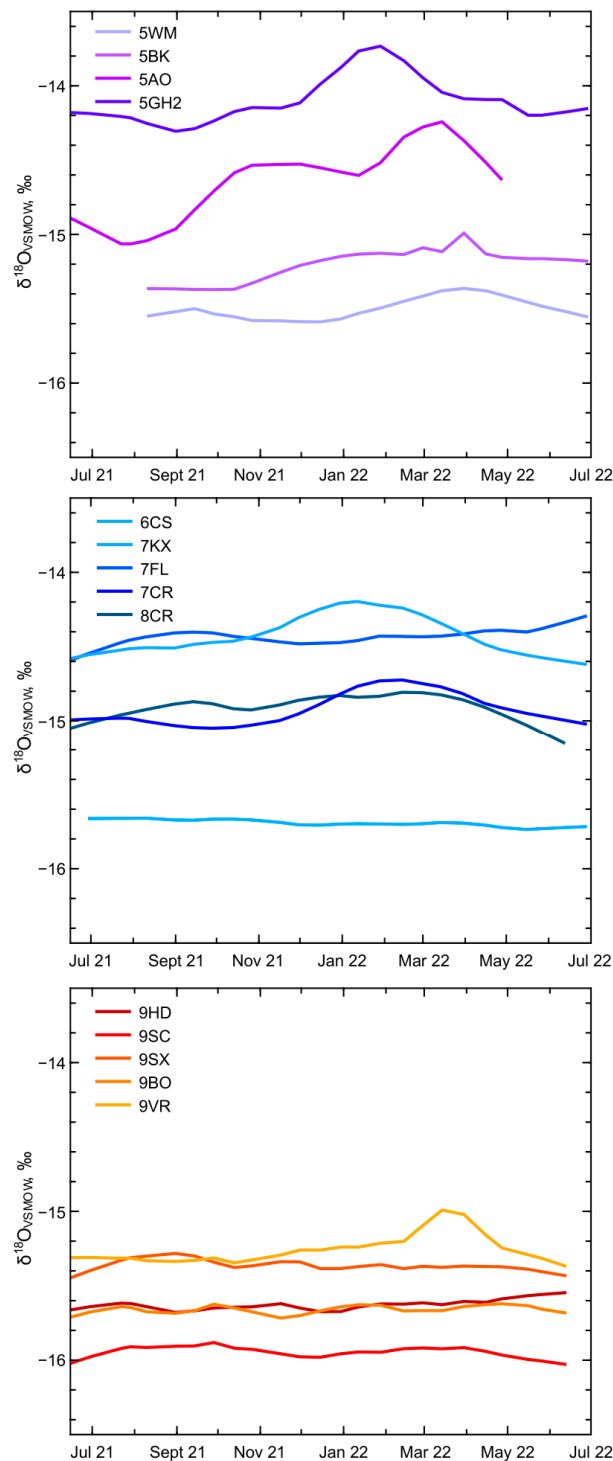


Figure 11. Lowest trend lines of mine water $\delta^{18}\text{O}$ values (grouped by mine level). Data missing from 5AO, 5WM, and 5BK because of limited accessibility.

3.3. Pyritic Zone Evaporation and Deuterium Excess

Evaluation of mine water $\delta^{18}\text{O}$ and d-excess values indicate that select upper-level sampling sites do not correspond to the potential upgradient source waters. Precipitation in the region can have low d-excess in the summer months; however, the volume of precipitation during this period is substantially lower and is subject to large evapotranspiration losses compared to the precipitation/snowmelt from late fall to spring (Figure 5) [40]. Snowfall in the study area is expected to have a relatively high d-excess that is greater with elevation [60]. The d-excess for precipitation collected by Sanchez-Murillo [40] in the Silver

Valley ranged from -10.5‰ to 21.0‰ , with the highest d-excess values in winter and the lowest in summer and early fall. The d-excess values (Figure 12) for this study's snowpack ranged from 6.2‰ to 14.7‰ , near the global average of 10‰ [61]. Higher elevation creek water (EMC and WMC) had d-excess values ranging from 7.7‰ to 17.7‰ , and lower elevation creek water (MMC) ranged from 7.9‰ to 16.6‰ . Water from the creek in Deadwood Gulch (DWG) indicated a d-excess range of 6.8‰ to 12.9‰ . The d-excess values for the mine water passing through the pyritic zone (low pH, high specific conductance (Levels 5 through 7)) ranged from -0.7‰ to 12.2‰ , while the d-excess values for the mine water that did not pass through the pyritic zone (high pH, low specific conductance) ranged from 4.5‰ to 19.6‰ . This d-excess difference between the inner and outer pyritic zone mine water suggests evaporation [40] and not an unidentified source water. The evaporation effect (approximate d-excess shift of 1.5‰ to 2.0‰) is visible between the inner and outer pyritic zone d-excess for the 5 Level (Figure 12). Given the likelihood of an evaporation effect in the pyritic zone, the source waters used to unmix the 5-Level pyritic zone sampling sites (5AO and 5GH2) require corrected source waters to account for this effect (1.5‰ for the DWG source water median value). Subsequent level unmixing required an additional source correction for the use of the inner pyritic zone water from the 5 Level (0.5‰ for the 5GH2 median value used as a source water).

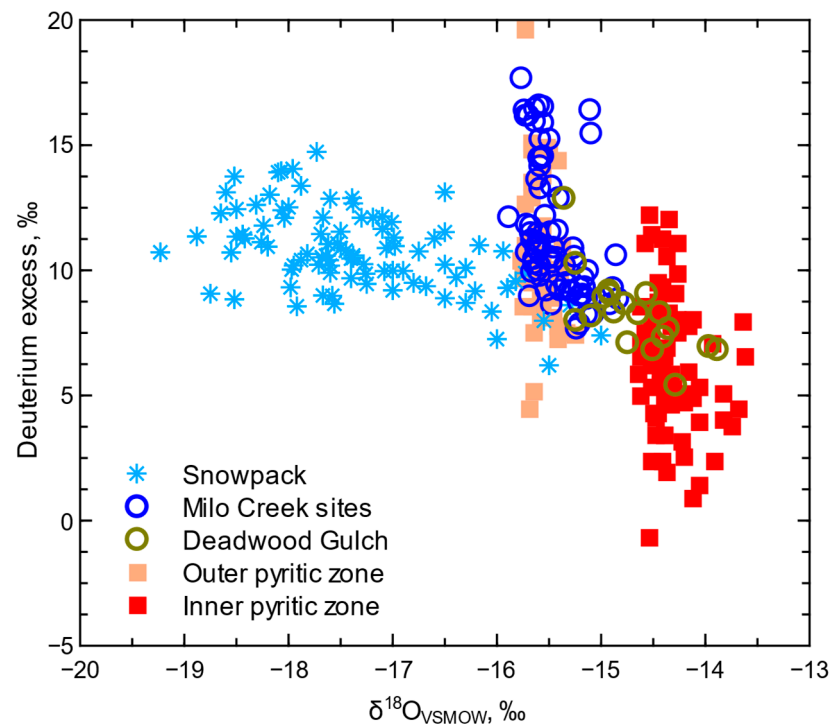


Figure 12. Distribution of deuterium excess and $\delta^{18}\text{O}$ for snowpack composite and basal layer samples (“Snowpack”), Deadwood Gulch and Milo Creek (MMC, EMC, and WMC) samples, mine water with dominant sources outside of the pyritic zone (outer pyritic zone sites of 5WM and 7KX), and mine water from the inner pyritic zone (5GH2, 6CS, and 7FL).

3.4. Source Water Unmixing

The field parameter and stable isotope results, along with information from prior investigations and observations during sample collection, were used to develop the conceptual model of the source waters and flowpaths in the upper workings of the mine (Figure 13). Given the hypothesized flowpaths, potential upgradient source waters (e.g., snowmelt, creek water, or upper-level mine water) were assigned to each sampling site given the possible two-component unmixing of each site's water with the source water $\delta^{18}\text{O}$ values (the two source-water $\delta^{18}\text{O}$ values had to encompass the mine site values). For 5-Level sites that contained $\delta^{18}\text{O}$ values more enriched than values recorded at any potential

source, the source water $\delta^{18}\text{O}$ value was set to the corrected $\delta^{18}\text{O}$ value determined by the d-excess analysis.

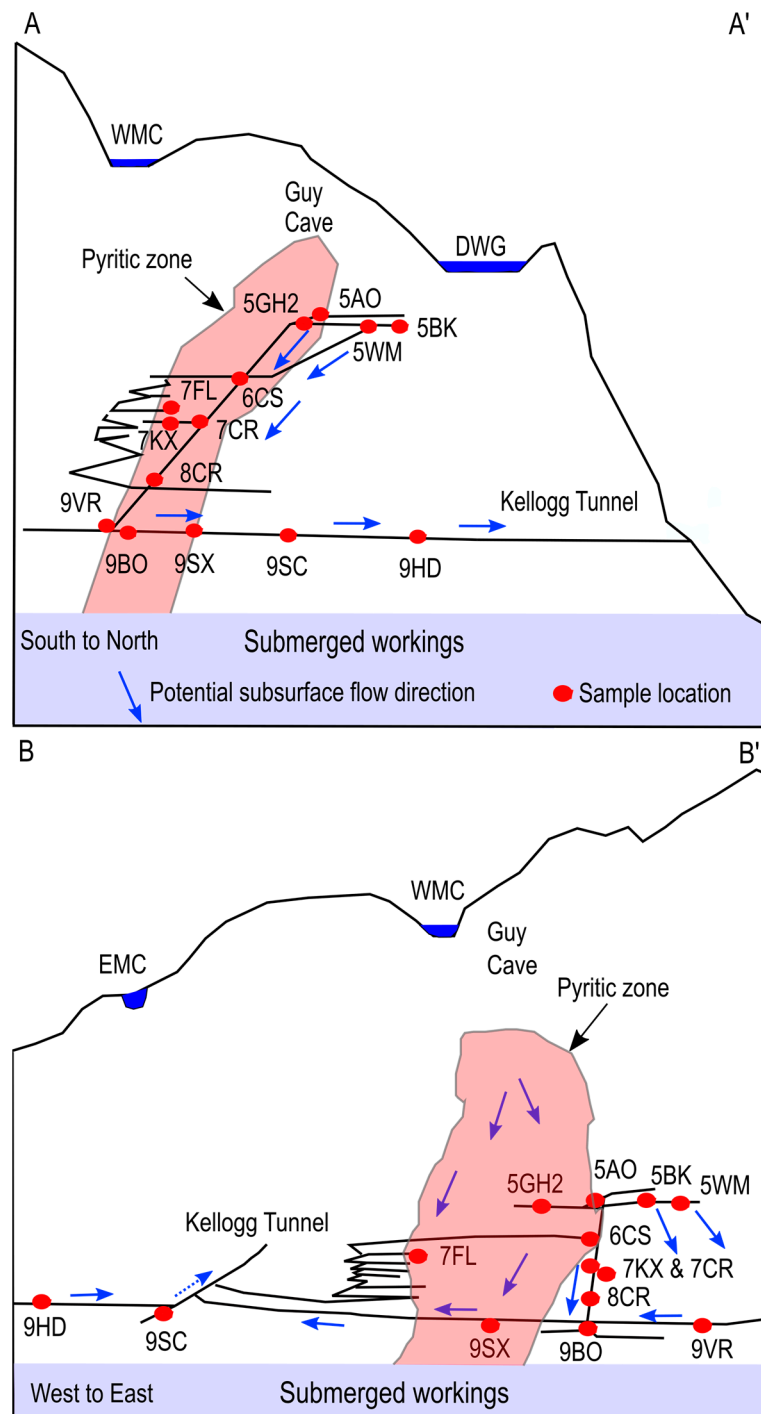


Figure 13. Simplified cross-sections (A–A', B–B' in Figure 4) of the mine workings depicting key features including the pyritic zone (position inferred), Guy Cave, overlying creeks, and potential flowpaths between levels and sites. West Milo Creek, East Milo Creek, and Deadwood Gulch are represented as WMC, EMC, and DWG, respectively. Adapted from Germon et al. [8] and LiDAR imaging of mine workings provided by Bunker Hill Mining Corporation.

Results of the $\delta^{18}\text{O}$ unmixing analysis (12 of the 14 mine sites shown in Figure 14) indicate that the mine receives multiple creek inflows along with a substantial infiltration of higher elevation snowmelt. Creek sources are dominant source waters at the 5 Level

and an increasing contribution of higher elevation snowmelt is present at certain sites, moving deeper into the mine. The two sites not included in Figure 14 (8CR and 9HD) had nearly identical unmixing results as 7CR (8CR) and 9BO (9HD). With a variable source contribution at the 5 Level and increased higher elevation snowmelt contributions deeper in the mine, the sampling sites can be split into two groups—sites with relatively stable contributions of the perceived source waters (e.g., 5WM, 7FL, 7KX, 9SX, 9BO (9HD), and 9SC) and sites that display temporally variable source-water contributions (5GH2, 5AO, 5BK, 6CS, 7CR (8CR), and 9VR). A temporal shift in source water contributions is reflective of the dominant recharge period that drives greater volumes of water into the mine, which increases flow in select pathways and may activate intermittent flowpaths. The timing of the shift in source water contributions is suggestive of the differences in travel times, such as the perceived early shift at 5GH2 and 6CS compared to the later shift at 5BK, 7CR (8CR), and 9VR. Mine water sites that exhibited the most stable source water contributions tended to contain higher elevation snowmelt (e.g., 5WM, 7KX, and 9SC), which is suggestive of the source water contributions dominated by snowmelt infiltration in the slower/longer flowpaths. More isotopically enriched mine water tended to exhibit more variation in source water contributions (e.g., 5GH2, 6CS, 7CR (8CR), and 9VR). These sites with variable source waters appear to be connected with the primary flowpath(s) connecting 5GH2, 6CS, 7CR (8CR), and 9VR.

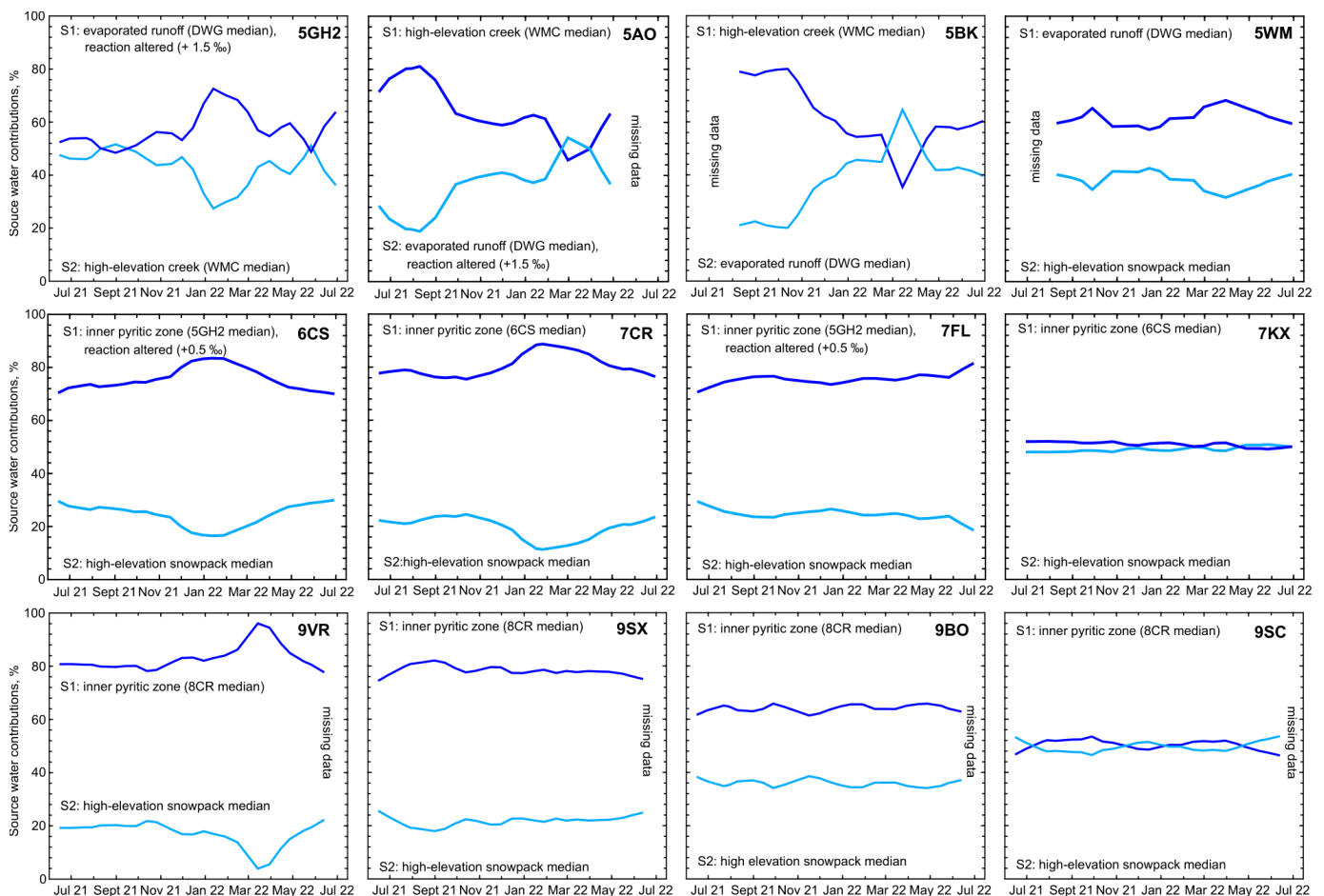


Figure 14. Lowest trend lines of source water contributions for select mine water sites derived from two-component (S1 and S2) unmixing of observed $\delta^{18}\text{O}$ values.

3.5. Mine Water Tritium and Relative Travel Time

Results of the ^3H analysis indicate a relative decrease in the median and distribution of ^3H concentrations with depth in the mine (Figure 15). Such a relative decrease is expected

with the degradation of ^3H during travel in the flowpaths that exceed the annual period. The snowpack and creeks contained water with higher ^3H concentrations, and Deadwood Gulch contained water with the highest ^3H median concentration. Sites 5BK, 7FL, and 9VR contained water with relatively higher ^3H distributions compared to other sites on those levels, which indicate the entrance of younger water. Correspondingly, relatively lower ^3H distributions were found in mine water at 5WM, 7KX, 9BO, and 9HD, which is indicative of older water entering these locations. The likely younger water present at 5BK and 9VR corresponds to the alteration in source dominance (Figure 14) that suggests the temporary inflow of younger water likely from seasonally active pathways, while the older water of 5WM, 7KX, and 9BO corresponds to steady source water contributions from longer flowpaths that minimize such variations (Figure 14).

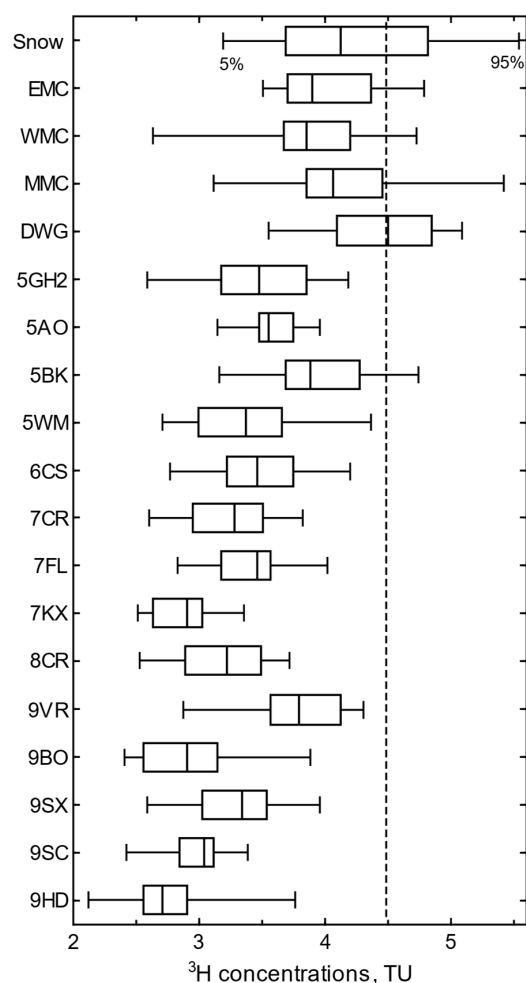


Figure 15. Boxplots of tritium values for snow (all sample sites), creek sites (EMC, WMC, MMC, and DWG), and all mine water sites. Only the 5% to 95% distribution is presented along with the 25–50–75% box. The dashed line is the selected $^3\text{H}_0$ value (DWG median, 62.5 percentile of the snowpack values, mean of the winter/spring (February to May) snowpack).

Travel time estimates for mine water ranged from <1 to 22 yr with most of the mine water samples indicating a potential travel time ≤ 10 yr (Figure 16). Mine water travel time estimates were relatively similar on the 5 to 8 Levels (<1 to 14 yr) with an increase in travel time range at the 9 Level (<1 to 22 yr). The increase in travel time at the 9 Level corresponds to the more depleted $\delta^{18}\text{O}$ values and lessening of the variability in $\delta^{18}\text{O}$ values (Figure 16). This lessening of $\delta^{18}\text{O}$ variability on the 9 Level also was present for mine water in the 6 to 8 Levels. The lower $\delta^{18}\text{O}$ variability in the samples from the 6 to 8 Levels did not correspond to a change in travel times that remained similar to estimates for the samples collected at

the 5 Level (Figure 16). A comparison of travel time estimates for the mine water from the 6 to 8 Levels indicates a slightly older, isotopically depleted source that appears on the 7 Level (7KX). The mixing of this older water that is a relative equal mix of higher elevation snowmelt and inner pyritic zone water (likely 6CS source water, Figure 14) further depletes the $\delta^{18}\text{O}$ signal and increases the travel time estimates. A similar effect is visible on the 9 Level at 9SC where a relatively older (and less variable) depleted isotope signal from the high elevation snowmelt mixes in near equal parts with the inner pyritic zone water (Figure 14), increases the median age, and compresses the travel time range compared to a more variable site such as 9VR (Figure 16).

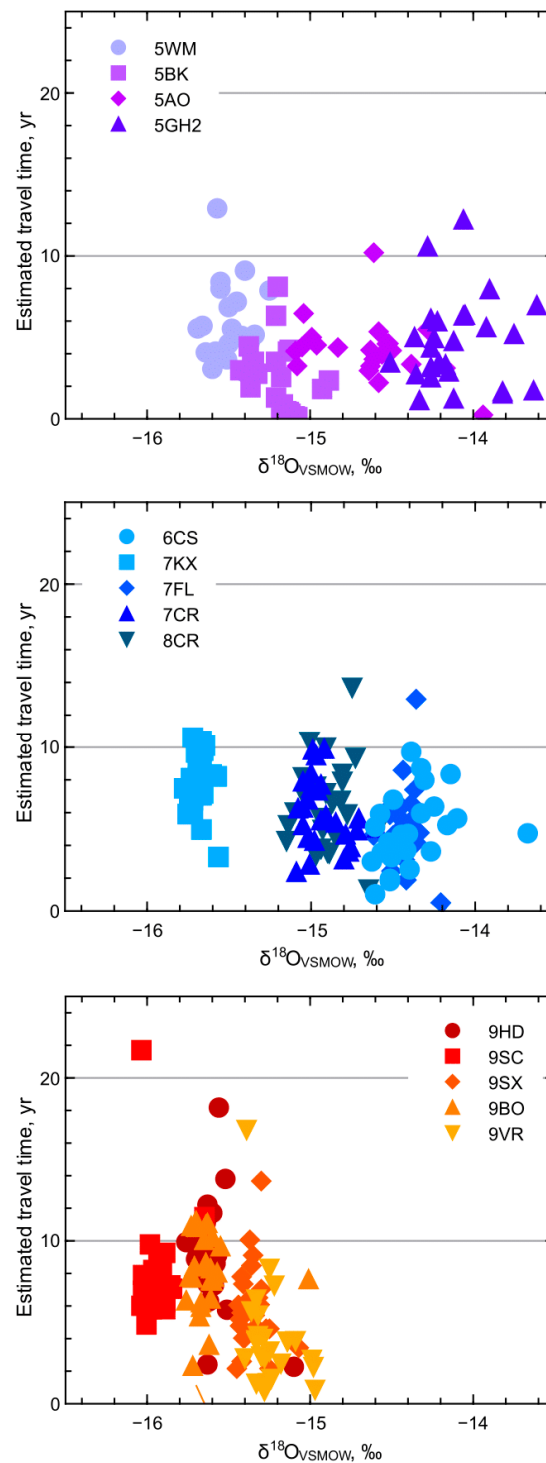


Figure 16. Estimated travel time and $\delta^{18}\text{O}$ of mine water sites.

4. Discussion

The anthropogenic and natural pathways for mine water produce two primary mine water types—lower elevation recharge in more temporally reactive flowpaths and higher elevation recharge in less reactive flowpaths (Figures 17 and 18). The lower elevation recharge corresponds to the anthropogenically-modified pathways that bring water to the 5 Level and allow for the substantial interaction with pyrite that produces the lowest pH (Figure 17). These pathways appear to contain water similar to the creeks in the Milo Creek and Deadwood Gulch watersheds (evolved overland runoff) and pass this water to the subsequent levels in the mine. This infiltrated creek water can intersect the pyritic zone, allowing for the enrichment of the stable-isotope signal through evaporation because of the exothermic oxidizing reactions. The higher elevation recharge likely is contained in more natural pathways (fractures, faults, and bedding planes) that bring the water to all levels of the mine with increasing contributions at each subsequent level in the mine. This higher elevation recharge to the mine water at all levels is indicated by the depletion shift of $\delta^{18}\text{O}$ that occurs with increasing depth in the mine, which has a corresponding shift (smaller) in ^3H concentrations (Figure 17). These increasing contributions from higher elevation recharge do not appear to have pathways that substantially intersect the upper-level workings and the pyritic zone.

Similar to the findings of Hartman [25], who suggested long and short pathways transporting water throughout the mine, the ^3H results from the current study indicate younger and older waters mixing on all mine levels (Figures 16 and 17). The greater contribution of higher elevation snowmelt with depth in the mine produces more depleted $\delta^{18}\text{O}$ values and slightly longer travel times (Figures 17 and 18). A subset of the samples indicated substantial increases in travel time for the mine water at the 9 Level. Although the anthropogenically modified pathways appear to allow for the greater infiltration of creek (young) water to the upper mine workings, the natural pathways that bring higher elevation snowmelt to each level of the mine are a mix of slow and faster pathways. These higher elevation pathways may have been enhanced by past mining that lessens the travel time of the water, which limits the increase in travel time (age).

The effect of the increasing contributions of higher elevation snowmelt that have not interacted with the pyritic zone is visible in the change in pH of the water coming from the inner pyritic zone. Sites that are primarily in the pyritic zone or receiving poor quality water from the pyritic zone include 5GH2, 5AO, 6CS, 7CR, 7FL, 8CR, and 9SX, which all had median pH values of <2.5. Assuming these sites are along a conduit of poor water quality that then mixes with water of a better quality (near-neutral pH and low conductance), the mixing improves the water quality and produces water such as the type observed at 9SC (Figures 14 and 17) with a median pH of 5.5. Without any mineralogical neutralization, an increase of pH from 2.5 to 5.5 would require a $>2\times$ dilution factor, which is near the source water contributions estimated for 9SC (Figure 14) that was predicted to receive approximately half of its water from the poor water conduit (8CR source) and half of its water from the higher elevation snowmelt that did not interact with the pyritic zone (SP5 source). This dilution effect was captured at 9SC, but it does not represent the discharge from the mine portal (Kellogg Tunnel, Figure 3), which typically has a pH of 3. Additionally, not all water received on the 9 Level will exit the mine portal and may continue deeper into the mine where a mine pool has formed below the 10 Level with a typical pH between 5 and 6.

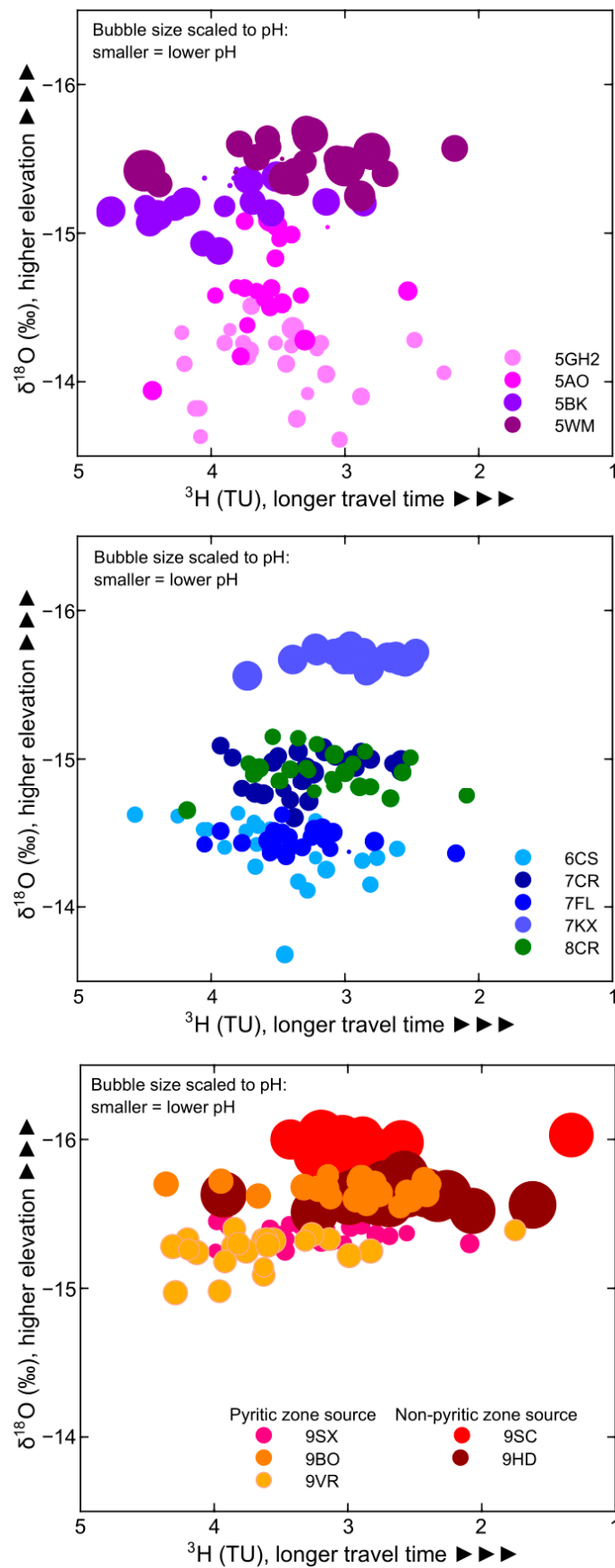


Figure 17. Tritium concentrations, $\delta^{18}\text{O}$ values, and pH for mine water sampling sites on each level with discrimination of sites in proximity or distant from the pyritic zone.

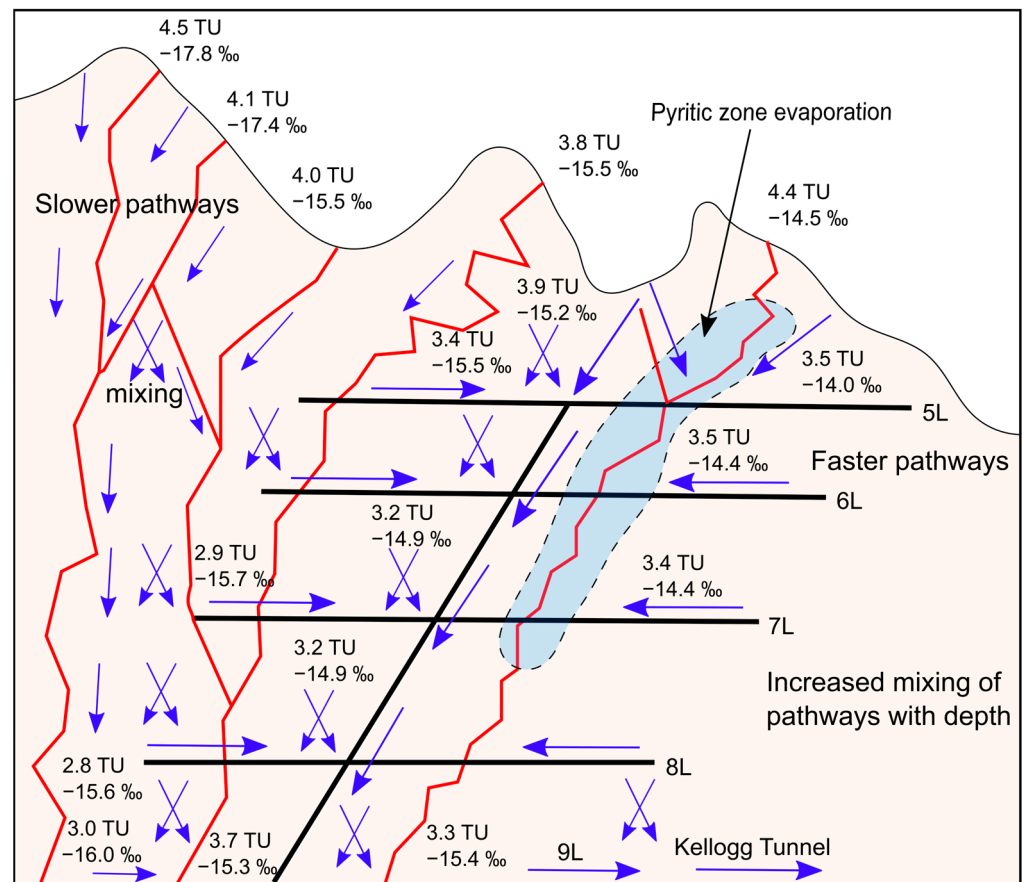


Figure 18. Simplified depiction of mine water sources and flowpaths in the Bunker Hill Mine with associated averages of ^3H and $\delta^{18}\text{O}$ values.

Past hydrogeologic studies at the mine have indicated a correlation of high flows in the Milo Creek Watershed with higher flows of mine water [7,16,23–25]. The 100+ yr of past mining has created anthropogenic pathways that increased mine water volumes, passing this water from level to level, and allowing for greater inflow from the natural pathways contained in faults, fractures, and bedding planes. With a future goal of reducing mine water discharge, the mine operator should pursue proposed activities of paste backfill in the upper mine workings, capping or source control in the Guy Cave area, and/or diversion of surface runoff (e.g., creek or other notable surface water features) near the perceived infiltration zones. The backfilling of the upper mine workings should reduce acid generation and minimize faster flowpaths from the lower elevation recharge that appears to be sourced from creek water. Capping or source control at the Guy Cave area will assist in reducing surface runoff in this area and remove the influence of the pyritic waste rock dumped in the Guy Cave depression. The reduction in surface water infiltration at the Guy Cave likely will reduce the mine water in the uppermost levels, and further source reduction in the Milo Creek Watershed should assist in minimizing these faster pathways into the upper mine workings. In addition to minimizing the inflows from the faster anthropogenically-modified pathways, source control outside of the pyritic zone likely will be necessary to reduce the higher elevation recharge and overall mine water discharge.

5. Summary and Conclusions

The complex geology, alteration from past mining, and large pyritic zone at the Bunker Hill Mine provide a heterogeneous environment that is producing acidic and neutral waters in the upper mine workings. The stable and radiogenic isotopes of water were used to identify the source waters derived from the snowmelt and overland flow in the surrounding

mountains. The snowpack samples contained relatively depleted $\delta^2\text{H}$ and $\delta^{18}\text{O}$ values and the largest ^3H values, providing baseline values for discriminating the source waters and their inflow into different levels of the mine. The upper elevation creek samples indicated variable but depleted $\delta^2\text{H}$ and $\delta^{18}\text{O}$ values, which became more enriched in the lower elevation creek samples. The spatial and temporal variation in the $\delta^2\text{H}$ and $\delta^{18}\text{O}$ values for the mine water were a product of the mixing of flowpaths from the higher elevation snowmelt, lower elevation infiltration areas that receive downslope runoff, and inflow from the upgradient mine levels. Select mine sites exhibited seasonal fluxes coinciding with the primary snowmelt period and associated shorter travel times and shifts in source water contributions. Upper-level sample sites in the pyritic zone responded relatively quickly to source water fluctuations, but these fluctuations decreased with depth in the mine. Source waters from high elevation infiltration zones appear to not substantially intersect the pyritic zone and are likely restricted to natural flowpaths, such as faults, fractures, and bedding planes. Once intercepted by mine-workings, mine water travels more quickly downgradient using the workings as primary flowpaths, as evident from the similar travel times observed on the 5 to 7 Levels. The higher elevation infiltrated waters have longer travel times and better water quality, often displaying less variation through time. Recommendations for reducing acidic discharge from the mine portal include paste backfill inside and outside the pyritic zone along with surface modifications in heavily fractured zones such as the Guy Cave area.

Supplementary Materials: The following supporting information can be downloaded at: <https://www.mdpi.com/article/10.3390/w15193362/s1>.

Author Contributions: Conceptualization, J.B.L. and B.B.; methodology, J.B.L., T.E.L., B.B. and M.H.; validation, J.B.L., T.E.L. and J.B.; formal analysis, J.B.L., E.G. and T.E.L.; investigation, J.B.L., E.G., B.B. and M.H.; resources, J.B.L., T.E.L., B.B. and M.H.; data curation, J.B.L., E.G. and M.H.; writing—original draft preparation, J.B.L. and E.G.; writing—review and editing, J.B.L., T.E.L., J.B., B.B. and M.H.; visualization, J.B.L., E.G., T.E.L. and J.B.; supervision, J.B.L., B.B. and M.H.; project administration, J.B.L., B.B. and M.H.; funding acquisition, J.B.L. and B.B. All authors have read and agreed to the published version of the manuscript.

Funding: This research was funded by the Bunker Hill Mining Corporation.

Data Availability Statement: All the data collected as part of this study can be found in the attached Supplementary Data File.

Acknowledgments: The authors wish to thank the Bunker Hill Mining Corporation for their support and funding of the study. The choice to conduct this study reflects the dedication of the Bunker Hill Mining Corporation to understand and minimize potential environmental impacts with the restart of mining activities at the site. Additionally, Karen Ryan, Environmental Technician, at the Bunker Hill Mining Corporation has been a key resource for the completion of the snow, surface water, and mine water sampling.

Conflicts of Interest: Although Bradley Barnett and Morgan Hill are part of the Bunker Hill Mining Corporation and the study was funded by the Bunker Hill Mining Corporation, personnel at the Bunker Hill Mining Corporation did not restrict the data availability, the data analysis, or the results interpretation and had no role in the decision to publish the results of the study.

References

1. Nordstrom, D.K.; Blowes, D.W.; Ptacek, C.J. Hydrogeochemistry and Microbiology of Mine Drainage: An Update. *Appl. Geochem.* **2015**, *57*, 3–16. [[CrossRef](#)]
2. Parbhakar-Fox, A.; Lottermoser, B. Principles of Sulfide Oxidation and Acid Rock Drainage. In *Environmental Indicators in Metal Mining*; Lottermoser, B., Ed.; Springer International Publishing: Cham, Switzerland, 2017; pp. 15–34, ISBN 978-3-319-42731-7.
3. Akcil, A.; Koldas, S. Acid Mine Drainage (AMD): Causes, Treatment and Case Studies. *J. Clean. Prod.* **2006**, *14*, 1139–1145. [[CrossRef](#)]
4. Gammons, C.H.; Metesh, J.J.; Duaiame, T.E. An Overview of the Mining History and Geology of Butte, Montana. *Mine Water Environ.* **2006**, *25*, 70–75. [[CrossRef](#)]

5. Daniels, W.; Orndorff, Z. Acid Rock Drainage from Highway and Construction Activities in Virginia, USA. In Proceedings of the 6th International Conference on Acid Rock Drainage, Cairns, QLD, Australia, 12–18 July 2003; pp. 479–487.
6. Egiebor, N.O.; Oni, B. Acid Rock Drainage Formation and Treatment: A Review. *Asia-Pac. J. Chem. Eng.* **2007**, *2*, 47–62. [[CrossRef](#)]
7. Lachmar, T.E. Application of Fracture-Flow Hydrogeology to Acid-Mine Drainage at the Bunker Hill Mine, Kellogg, Idaho. *J. Hydrol.* **1994**, *155*, 125–149. [[CrossRef](#)]
8. Germon, M.; Stefanoff, J.; Riley, J.; Hudson, B. *Acid Mine Drainage—Bunker Hill Mine Water Conceptual Model*; CH2M Hill: Englewood, CO, USA, 1999.
9. Umpleby, J.B.; Jones, E.L. *Geology and Ore Deposits of Shoshone County, Idaho*; Bulletin 732; U.S Geological Survey 778; U.S Geological Survey: Reston, VA, USA, 1923. [[CrossRef](#)]
10. Box, S.E.; Bookstrom, A.A.; Anderson, R.G. Origins of Mineral Deposits, Belt-Purcell Basin, United States and Canada: An Introduction. *Econ. Geol.* **2012**, *107*, 1081–1088. [[CrossRef](#)]
11. Fleck, R.J.; Criss, R.E.; Eaton, G.F.; Cleland, R.W.; Wavra, C.S.; Bond, W.D. Age and Origin of Base and Precious Metal Veins of the Coeur D’Alene Mining District, Idaho. *Econ. Geol.* **2002**, *97*, 23–42. [[CrossRef](#)]
12. Ferraro, J.M. Relationships between Deformation and Mesothermal Veins in the Sunshine Mine Area, Coeur d’Alene District, Idaho. Master’s Thesis, University of Iowa, Iowa City, IA, USA, 2013. [[CrossRef](#)]
13. Mauk, J. *Stratigraphy of the Proterozoic Revett Formation, Coeur d’Alene District, Idaho*; Open-File Report 01-319; U.S Geological Survey: Reston, VA, USA, 2002. Available online: <https://pubs.usgs.gov/of/2001/of01-319/> (accessed on 30 July 2023).
14. Hunt, J. *Analysis of Recharge to an Underground Lead-Zinc Mine, Coeur D’Alene Mining District, Idaho*; Idaho Bureau of Mines and Geology: Moscow, ID, USA, 1984.
15. Umpleby, J.B. The Osburn Fault, Idaho. *J. Geol.* **1924**, *32*, 601–614. [[CrossRef](#)]
16. Lachmar, T.E. The Influence of Fracture Properties on Ground-Water Flow at the Bunker Hill Mine, Kellogg, Idaho. *Environ. Eng. Geosci.* **1993**, *4*, 395–407. [[CrossRef](#)]
17. Mauk, J.L.; White, B.G. Stratigraphy of the Proterozoic Revett Formation and Its Control on Ag-Pb-Zn Vein Mineralization in the Coeur d’Alene District, Idaho. *Econ. Geol.* **2004**, *99*, 295–312. [[CrossRef](#)]
18. Balistrieri, L.S.; Box, S.E.; Bookstrom, A.A.; Ikramuddin, M. Assessing the Influence of Reacting Pyrite and Carbonate Minerals on the Geochemistry of Drainage in the Coeur d’Alene Mining District. *Environ. Sci. Technol.* **1999**, *33*, 3347–3353. [[CrossRef](#)]
19. Riley, J.A.; Erikson, D.L.; Ralston, D.R.; Williams, R.E. The Hydrogeology of an Underground Lead-Zinc Mine: Water Flow and Quality Characteristics. *Int. J. Mine Water* **1984**, *3*, 39–53. [[CrossRef](#)]
20. Erikson, D.L. Analysis of Water Movement in an Underground Lead-Zinc Mine, Coeur D’Alene Mining District, Idaho. Master’s Thesis, University of Idaho, Moscow, ID, USA, 1985.
21. Serreze, M.C.; Clark, M.P.; Armstrong, R.L.; McGinnis, D.A.; Pulwarty, R.S. Characteristics of the Western United States Snowpack from Snowpack Telemetry Data. *Water Resour. Res.* **1999**, *35*, 2145–2160. [[CrossRef](#)]
22. Rozanski, K.; Gonfiantini, R.; Araguas-Araguas, L. Tritium in the Global Atmosphere: Distribution Patterns and Recent Trends. *J. Phys. G Nucl. Part. Phys.* **1991**, *17*, S523–S536. [[CrossRef](#)]
23. Trexler, B.D., Jr.; Ralston, D.R.; Reecs, D.R.; Williams, R.E. *Sources and Causes of Acid Mine Drainage*; Idaho Bureau of Mines and Geology: Moscow, ID, USA, 1975.
24. Wai, C.M.; Reece, D.E.; Trexler, B.D.; Ralston, D.R.; Williams, R.E. Production of Acid Water in a Lead-Zinc Mine, Coeur d’Alene, Idaho. *Geo* **1980**, *3*, 159–162. [[CrossRef](#)]
25. Hartman, M. A Study of Groundwater Age in the Bunker Hill Mine. Master’s Thesis, University of Idaho, Moscow, ID, USA, 1986.
26. Birkel, C.; Soulsby, C. Advancing Tracer-Aided Rainfall–Runoff Modelling: A Review of Progress, Problems and Unrealised Potential. *Hydrol. Process.* **2015**, *29*, 5227–5240. [[CrossRef](#)]
27. Cartwright, I.; Morgenstern, U. Using Tritium and Other Geochemical Tracers to Address the “Old Water Paradox” in Headwater Catchments. *J. Hydrol.* **2018**, *563*, 13–21. [[CrossRef](#)]
28. Cauquoin, A.; Jean-Baptiste, P.; Risi, C.; Fourré, É.; Stenni, B.; Landais, A. The Global Distribution of Natural Tritium in Precipitation Simulated with an Atmospheric General Circulation Model and Comparison with Observations. *Earth Planet. Sci. Lett.* **2015**, *427*, 160–170. [[CrossRef](#)]
29. Faure, G. *Principles of Isotope Geology*, 2nd ed.; John Wiley & Sons: Hoboken, NJ, USA, 1986; ISBN 0471864129.
30. Gat, J.R. Oxygen and Hydrogen Isotopes in the Hydrologic Cycle. *Annu. Rev. Earth Planet. Sci.* **1996**, *24*, 225–262. [[CrossRef](#)]
31. Beria, H.; Larsen, J.R.; Ceperley, N.C.; Michelon, A.; Vennemann, T.; Schaefli, B. Understanding Snow Hydrological Processes through the Lens of Stable Water Isotopes. *WIREs Water* **2018**, *5*, e1311. [[CrossRef](#)]
32. Galewsky, J.; Steen-Larsen, H.C.; Field, R.D.; Worden, J.; Risi, C.; Schneider, M. Stable Isotopes in Atmospheric Water Vapor and Applications to the Hydrologic Cycle. *Rev. Geophys.* **2016**, *54*, 809–865. [[CrossRef](#)] [[PubMed](#)]
33. Moser, H.; Stichler, W. Deuterium and Oxygen-18 Contents as an Index of the Properties of Snow Covers. *Int. Assoc. Hydrol. Sci.* **1974**, *114*, 122–135.
34. Zongxing, L.; Qi, F.; Wei, L.; Tingting, W.; Xiaoyan, G.; Zongjie, L.; Yan, G.; Yanhui, P.; Rui, G.; Bing, J.; et al. The Stable Isotope Evolution in Shiyi Glacier System during the Ablation Period in the North of Tibetan Plateau, China. *Quat. Int.* **2015**, *380–381*, 262–271. [[CrossRef](#)]

35. Earman, S.; Campbell, A.R.; Phillips, F.M.; Newman, B.D. Isotopic Exchange between Snow and Atmospheric Water Vapor: Estimation of the Snowmelt Component of Groundwater Recharge in the Southwestern United States. *J. Geophys. Res. Atmos.* **2006**, *111*. [[CrossRef](#)]
36. Jasechko, S.; Perrone, D.; Befus, K.M.; Bayani Cardenas, M.; Ferguson, G.; Gleeson, T.; Luijendijk, E.; McDonnell, J.J.; Taylor, R.G.; Wada, Y.; et al. Global Aquifers Dominated by Fossil Groundwaters but Wells Vulnerable to Modern Contamination. *Nat. Geosci.* **2017**, *10*, 425–429. [[CrossRef](#)]
37. Winograd, I.J.; Riggs, A.C.; Coplen, T.B. The Relative Contributions of Summer and Cool-Season Precipitation to Groundwater Recharge, Spring Mountains, Nevada, USA. *Hydrogeol. J.* **1998**, *6*, 77–93. [[CrossRef](#)]
38. Xi, X. A Review of Water Isotopes in Atmospheric General Circulation Models: Recent Advances and Future Prospects. *Int. J. Atmos. Sci.* **2014**, *2014*, e250920. [[CrossRef](#)]
39. Xu, Q.; Hoke, G.D.; Liu-Zeng, J.; Ding, L.; Wang, W.; Yang, Y. Stable Isotopes of Surface Water across the Longmenshan Margin of the Eastern Tibetan Plateau. *Geochem. Geophys. Geosyst.* **2014**, *15*, 3416–3429. [[CrossRef](#)]
40. Sánchez-Murillo, R.; Brooks, E.S.; Elliot, W.J.; Boll, J. Isotope Hydrology and Baseflow Geochemistry in Natural and Human-Altered Watersheds in the Inland Pacific Northwest, USA. *Isot. Environ. Health Stud.* **2015**, *51*, 231–254. [[CrossRef](#)]
41. Ansari, M.A.; Mohokar, H.V.; Deodhar, A.; Jacob, N.; Sinha, U.K. Distribution of Environmental Tritium in Rivers, Groundwater, Mine Water and Precipitation in Goa, India. *J. Environ. Radioact.* **2018**, *189*, 120–126. [[CrossRef](#)]
42. Geyh, M.A.; Schleicher, H. *Absolute Age Determination: Physical and Chemical Dating Methods and Their Application*; Springer Science & Business Media: Berlin/Heidelberg, Germany, 2012; ISBN 978-3-642-74826-4.
43. Craig, H.; Lal, D. The Production Rate of Natural Tritium. *Tellus* **1961**, *13*, 85–105. [[CrossRef](#)]
44. Zahn, A.; Barth, V.; Pfeilsticker, K.; Platt, U. Deuterium, Oxygen-18, and Tritium as Tracers for Water Vapour Transport in the Lower Stratosphere and Tropopause Region. *J. Atmos. Chem.* **1998**, *30*, 25–47. [[CrossRef](#)]
45. Harms, P.A.; Visser, A.; Moran, J.E.; Esser, B.K. Distribution of Tritium in Precipitation and Surface Water in California. *J. Hydrol.* **2016**, *534*, 63–72. [[CrossRef](#)]
46. Michel, R.L.; Jurgens, B.C.; Young, M.B. *Tritium Deposition in Precipitation in the United States, 1953–2012*; Scientific Investigations Report 2018–5086; U.S. Geological Survey: Reston, VA, USA, 2018; p. 19. [[CrossRef](#)]
47. Visser, A.; Thaw, M.; Esser, B. Analysis of Air Mass Trajectories to Explain Observed Variability of Tritium in Precipitation at the Southern Sierra Critical Zone Observatory, California, USA. *J. Environ. Radioact.* **2018**, *181*, 42–51. [[CrossRef](#)] [[PubMed](#)]
48. Lu, F.H. How Long Is Enough: CO₂-H₂O Equilibration for δ¹⁸O Analysis in Saline Formation Waters? *Rapid Commun. Mass Spectrom.* **2016**, *30*, 1647–1652. [[CrossRef](#)]
49. Lucas, L.L. Massic Activity Ratios of the NBS/NIST Tritiated-Water Standards Issued Between 1954 and 1999. *J. Res. Natl. Inst. Stand. Technol.* **2000**, *105*, 535–539. [[CrossRef](#)] [[PubMed](#)]
50. Dansgaard, W. Stable Isotopes in Precipitation. *Tellus* **1964**, *16*, 436–468. [[CrossRef](#)]
51. Langman, J.B.; Martin, J.; Gaddy, E.; Boll, J.; Behrens, D. Snowpack Aging, Water Isotope Evolution, and Runoff Isotope Signals, Palouse Range, Idaho, USA. *Hydrology* **2022**, *9*, 94. [[CrossRef](#)]
52. Peng, H.; Mayer, B.; Norman, A.L.; Krouse, H.R. Modelling of Hydrogen and Oxygen Isotope Compositions for Local Precipitation. *Tellus B Chem. Phys. Meteorol.* **2005**, *57*, 273. [[CrossRef](#)]
53. Kong, Y.; Pang, Z.; Froehlich, K. Quantifying Recycled Moisture Fraction in Precipitation of an Arid Region Using Deuterium Excess. *Tellus B Chem. Phys. Meteorol.* **2013**, *65*, 19251. [[CrossRef](#)]
54. Lucas, L.L.; Unterwieser, M.P. Comprehensive Review and Critical Evaluation of the Half-Life of Tritium. *J. Res. Natl. Inst. Stand. Technol.* **2000**, *105*, 541–549. [[CrossRef](#)] [[PubMed](#)]
55. Kalbus, E.; Reinstorf, F.; Schirmer, M. Measuring Methods for Groundwater–Surface Water Interactions: A Review. *Hydrol. Earth Syst. Sci.* **2006**, *10*, 873–887. [[CrossRef](#)]
56. Dos Santos, E.C.; de Mendonça Silva, J.C.; Duarte, H.A. Pyrite Oxidation Mechanism by Oxygen in Aqueous Medium. *J. Phys. Chem. C* **2016**, *120*, 2760–2768. [[CrossRef](#)]
57. Warren, J.W. Ventilation Report of Bunker Hill and Sullivan Mine Kellogg, Idaho. Master’s Thesis, Montana Tech. The University of Montana, Butte, MT, USA, 1950.
58. Winterhalder, K. Reclamation of Smelter-Damaged Lands. In *Reclamation of Drastically Disturbed Lands*; John Wiley & Sons, Ltd.: Hoboken, NJ, USA, 2000; pp. 819–853, ISBN 978-0-89118-233-7.
59. Siegel, F.R. Heavy Metals Mobility/Immobility in Environmental Media. In *Environmental Geochemistry of Potentially Toxic Metals*; Siegel, F.R., Ed.; Springer: Berlin/Heidelberg, Germany, 2002; pp. 45–59, ISBN 978-3-662-04739-2.
60. Bershaw, J.; Hansen, D.D.; Schauer, A.J. Deuterium Excess and ¹⁷O-Excess Variability in Meteoric Water across the Pacific Northwest, USA. *Tellus B Chem. Phys. Meteorol.* **2020**, *72*, 1773722. [[CrossRef](#)]
61. Craig, H. Isotopic Variations in Meteoric Waters. *Science* **1961**, *133*, 1702–1703. [[CrossRef](#)] [[PubMed](#)]

Disclaimer/Publisher’s Note: The statements, opinions and data contained in all publications are solely those of the individual author(s) and contributor(s) and not of MDPI and/or the editor(s). MDPI and/or the editor(s) disclaim responsibility for any injury to people or property resulting from any ideas, methods, instructions or products referred to in the content.